Available online at www.sciencedirect.com
SCIENCE DIRECT®
Polymer 45 (2004) 2357–2366
polymer
www.elsevier.com/locate/polymer

Experimental characterisation and further molecular modelling of the conformational and elastic behaviour of poly(ethylene terephthalate) network chains

L.S. Saunders[a], I.M. Ward[a,*], J.I. Cail[b], R.F.T. Stepto[b]

[a]*IRC in Polymer Science and Technology, School of Physics and Astronomy, University of Leeds, Woodhouse Lane, Leeds LS2 9JT, UK*
[b]*Polymer Science and Technology Group, Manchester Materials Science Centre, UMIST and University of Manchester, Grosvenor Street, Manchester M1 7HS, UK*

Received 15 September 2003; accepted 19 January 2004

Abstract

The Monte-Carlo (MC) method developed to model the elastomeric stress–strain behaviour of polyethylene (PE), poly(dimethyl siloxane) (PDMS) and poly(ethylene terephthalate) (PET) networks and the stress-optical behaviour of PE networks is now developed to investigate further the stress–strain behaviour of PET networks. Accurate infrared (IR) spectrometry measurements have been used to determine the populations of *gauche* conformers in the glycol residues of PET chains in melts. The proportion of *gauche* states was found to be 76%, consistent with the rotational energy difference of -4.16 kJ mol^{-1} between *trans* and *gauche* states used previously.

The greater conformational flexibility of the PET chain compared with the PE chain leads to lower network moduli and smaller deviations from Gaussian and affine network behaviour. Previous results are briefly reviewed and new comparisons of the elastic behaviour of PET and PE chains are made using normalised plots. Subsequent publications will apply the present results to interpreting the measured stress–strain and the stress-optical properties of entangled PET melts.

Keywords: Stress–strain behaviour; C–C bond; Poly(ethylene terephthalate) network chains

1. Introduction

It has been shown previously [1,2] that the conformational behaviour of poly(ethylene terephthalate) (PET) chains in melts does not follow the Williams–Flory (W–F) rotational-isomeric-state (RIS) model [3]. That model was derived to describe the conformational behaviour in mixed phenol solvents. A new RIS model with a much lower energy for the *gauche* conformation about the C–C bond of the glycol segment is needed for melts [2]. In the present paper, this RIS model is investigated further using new results from infrared (IR) spectrometry measurements of conformer populations. The model is then used in MC network calculations to simulate the stress–strain behaviour of networks of PET chains.

* Corresponding author. Tel.: +44-343-2333808; fax: +44-113-3433809.
E-mail address: i.m.ward@leeds.ac.uk (I.M. Ward).

0032-3861/$ - see front matter © 2004 Elsevier Ltd. All rights reserved.
doi:10.1016/j.polymer.2004.01.044

2. Geometry of the PET chain

The *trans*-terephthaloyl and *cis*-terephthaloyl isomers of the six-bond repeat-unit structure used are shown in Fig. 1. The geometrical parameters (bond lengths, l_i, and valence angle supplements, θ_i) taken from Williams and Flory [3], are as follows: $l_1 = l_3 = l_{O-C'} = 0.134$ nm (C′ denotes the carbonyl carbon atom), $l_4 = l_6 = l_{O-C} = 0.144$ nm, $l_5 = l_{C-C} = 0.153$ nm, $l_2 = 0.574$ nm (virtual bond), $\theta_1 = \theta_2 = 66°$, $\theta_3 = \theta_6 = 67°$, and $\theta_4 = \theta_5 = 70°$.

3. Conformational properties of the RIS chain model and PET chains in melts

3.1. Characteristic ratio

The characteristic ratio $(\langle r^2\rangle/M)_\infty$ for linear PET chains in bulk, obtained by Gilmer et al. [4] from neutron scattering

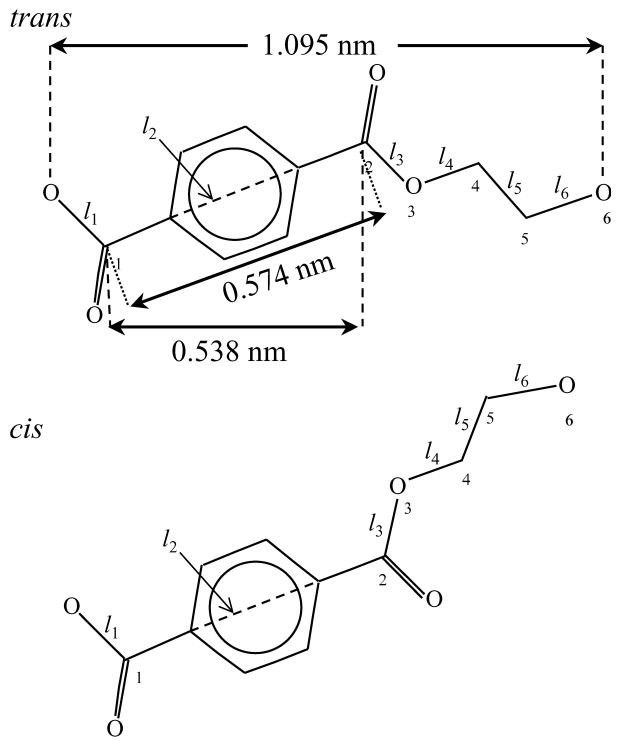

Fig. 1. *Trans* and *cis* PET repeat-unit structures, after Williams and Flory[3]; skeletal atoms are labelled 1–6, and the *i*th bond connects pairs of atoms with indices i and $i-1$; bond lengths are denoted l_i. The fully extended length of the *trans* repeat unit is 1.095 nm. The length of the virtual bond spanning the aromatic ring is 0.574 nm and its length resolved along the direction of the fully extended *trans* repeat unit is 0.538 nm.

measurements at 523 K, has been determined as 6.14×10^{-3} or 6.94×10^{-3} nm^2 using Guinier and Kratky analyses, respectively. These values may be contrasted with that of 10.5×10^{-3} nm^2 evaluated from the intrinsic viscosity measurements quoted by Williams and Flory [3] for a phenol–trichlorophenol solvent mixture at 303 K.

3.2. C–C bond conformer population

A review [2] of published values [5–11] for the proportion of *gauche* states about the C–C bond (bond 5 in Fig. 1) gave a range from 75 to 88%. This range was not deemed to be satisfactory, especially as some of the values were quoted as having uncertainties of ±5%. The proportion of *gauche* states has therefore been carefully measured again in the present work using IR spectrometry.

A single beam BOMEM FTIR spectrometer was used to measure the absorbance, A, of infrared radiation by isotropic PET film as a function of wavenumber. Polarised radiation was used to determine the absorbance both parallel with and perpendicular to a reference direction in the film. This was set at 45° to the vertical in order to eliminate the effects of any inherent beam polarisation. The spectra were compared to a reference spectrum obtained when the spectrometer was run with no sample in place.

The spectra were adjusted so that the apparent baseline coincided with $A = 0$. The data were then corrected for the effects of imperfect polarisers. A perfect polariser would let through all radiation that was oriented such that the electric vector is parallel to the polariser's preferred direction, i.e. the fraction of this radiation transmitted, T_1, is 1. Similarly a perfect polariser would absorb all perpendicular radiation, and so the fraction of radiation transmitted in this direction, T_2, is 0. The transmission, T, is related to the absorbance, A by

$$A = \log_{10}\left(\frac{1}{T}\right). \tag{1}$$

Real polarisers are not perfect and so T_1 is somewhat less than 1 and T_2 is greater than 0. Green and Bower [12] have shown that the values of T_1 and T_2 may be determined by studying the spectra obtained when two identical polarisers are placed in the IR radiation beam. Although two real polarisers are never precisely identical, the difference between their values of T_1, say, will be far less than the difference between T_1 and the theoretical value of 1. Spectra were recorded with two polarisers first parallel and then perpendicular to each other. This technique also eliminates any errors that may occur due to the spectrometer having different sensitivities to radiation polarised in different directions. The values of T_1 and T_2 were determined for the polariser used in this work and found to remain reasonably constant over the wavenumber range used. The experimentally obtained spectra were then corrected for the effects described, following the somewhat involved procedure given by Green and Bower [12].

The corrected spectra were studied using Thermo Galactic software [13]. This enabled a theoretical spectrum, consisting of 41 individual peaks, to be generated. The initial positions of the peaks were chosen using the range of values quoted by previous workers in this laboratory [14–17]. Most notably Yazdanian, Ward and Brody [14] introduced several new peaks compared to earlier workers, and confirmed their existence by carefully checking the spectra of model polyester compounds. In addition, three new peaks were included in the analysis of the current data at the high wavenumber end of the spectrum, in order to fit the tail of the data. The position and halfwidth of each peak were allowed to vary by a few wavenumbers, and the height of each was initially left unrestrained. The shape of each peak was allowed to vary between those of Gaussian and Lorentzian curves. A minimisation process then fitted the master theoretical curve to the experimental data. This process generated values of the position, the height and the area, a, of each constituent peak. The two sets of data, obtained with the polarised radiation being parallel and then perpendicular to the reference direction of the sample, gave areas $a_{\parallel}$ and $a_{\perp}$, respectively.

Some of the radiation emitted by the source will be lost due to reflection from the surface of the sample, increasing the apparent absorbance. The absorbance will also be dependant on the thickness of the sample and the

wavenumber. Abell [18] showed that the true absorbances, $k_{\|}$ and $k_{\perp}$, may be determined from the areas under the peaks using the equations

$$k_{\|} = \frac{a_{\|}\lambda}{0.4343 \times 4 \times \pi \times t} \qquad k_{\perp} = \frac{a_{\perp}\lambda}{0.4343 \times 4 \times \pi \times t} \quad (2)$$

where t is the thickness of the sample and λ is the wavelength at the centre of the peak.

The electric field experienced by the dipoles of the material will differ from the applied field due to the effects of neighbouring molecules, the so-called internal field effect. Cunningham, Davies and Ward [19] approximate this internal field to a Lorentz field, and hence determine a corrected absorbance, ϕ, which for low absorbances is given by

$$\phi_{\|} = \frac{6n_3k_{\|}}{(n_3+2)^2} \qquad \phi_{\perp} = \frac{6n_1k_{\perp}}{(n_1+2)^2} \quad (3)$$

where n_3 and n_1 are the refractive indices parallel and perpendicular to the reference direction in the film, respectively. The total absorbance at a particular wavenumber is then given by

$$\phi = \frac{1}{3}(\phi_{\|} + 2\phi_{\perp}) \quad (4)$$

Following previous workers [20–22], the glycol segment C–C conformer population can be determined from the IR spectra. The total *trans* content is taken as the sum of the areas of the peaks at 963, 972 and 978 cm^{-1}, and the total *gauche* content as the sum of the areas of the 890, 899 and 906 cm^{-1} peaks. It is assumed that the *trans* and *gauche* conformers have identical extinction coefficients, so the sum of the peak areas is constant; this assumption has been shown to be valid for PET [23].

Two methods were employed to determine the reliability of the results obtained in this work. First of all, as the designation of 'parallel' and 'perpendicular' is arbitrary in an isotropic material, the data were re-analysed with the opposite designation. Secondly, four different master curves containing slightly different values of the position, height and area of each constituent peak were used as the starting point for the curve fitting procedure. The combination of the various results obtained showed that the proportion of *gauche* states about the C–C bond in the glycol segment was 76 ± 1%. It should be noted that this proportion comes from measurements using melt-extruded PET film quenched to room temperature, well below the T_g of the polymer. The conformer population therefore relates most closely to the melt temperature. Information received from DuPont UK Ltd indicates that this temperature is somewhere in the range 260–280 °C (533–553 K).

4. RIS model

As described previously [1,2], the RIS treatment considers probabilities associated with the rotational states of consecutive pairs of skeletal bonds. The statistical weight, $u_{\eta\zeta;i}$ associated with a rotational state η of skeletal bond i is also dependent upon the state ζ at bond $i-1$. The value of $u_{\eta\zeta;i}$ is related to the corresponding rotational energy, $E_{\eta\zeta;i}$, by

$$u_{\eta\zeta;i} = \exp\left(\frac{-E_{\eta\zeta;i}}{RT}\right). \quad (5)$$

The set of interdependent statistical weights pertaining to all rotational states for a given bond pair can be expressed in the form of a statistical weights matrix $U_i = [u_{\eta\zeta;i}]$, with states ζ for bond $i-1$ indexing the rows and states η for bond i indexing the columns. The statistical weights matrices for the six skeletal bonds of the PET repeat unit (see Fig. 1) are listed in the following equations [1].

$$i \neq 2,3;\ U_i = \begin{bmatrix} & g_- & t & g_+ \\ g_- & & & \\ t & & & \\ g_+ & & & \end{bmatrix};$$

$$U_2 = \begin{bmatrix} & cis & trans \\ g_- & & \\ t & & \\ g_+ & & \end{bmatrix}; U_3 = \begin{bmatrix} & g_- & t & g_+ \\ cis & & & \\ trans & & & \end{bmatrix}$$

$$U_1 = \begin{bmatrix} 0 & 1 & 0 \\ 0 & 1 & 0 \\ 0 & 1 & 0 \end{bmatrix} \quad (6)$$

$$U_2 = \begin{bmatrix} 0 & 0 \\ 1 & 1 \\ 0 & 0 \end{bmatrix} \quad (7)$$

$$U_3 = \begin{bmatrix} 0 & 1 & 0 \\ 0 & 1 & 0 \end{bmatrix} \quad (8)$$

$$U_4 = \begin{bmatrix} 0 & 0 & 0 \\ \sigma_4 & 1 & \sigma_4 \\ 0 & 0 & 0 \end{bmatrix} \quad (9)$$

$$U_5 = \begin{bmatrix} \sigma_5 & 1 & \sigma_5\omega \\ \sigma_5 & 1 & \sigma_5 \\ \sigma_5\omega & 1 & \sigma_5 \end{bmatrix} \quad (10)$$

$$U_6 = \begin{bmatrix} \sigma_6 & 1 & \sigma_6\omega \\ \sigma_6 & 1 & \sigma_6 \\ \sigma_6\omega & 1 & \sigma_6 \end{bmatrix} \quad (11)$$

The model has *gauche* conformational states of bonds 4, 5, and 6 at $\phi_{g\pm} = \pm 120°$.

5. Choice of the C–C *gauche* energy ($E_{\sigma 5}$)

The value of $E_{\sigma 5}$ needs to be chosen so that $(\langle r^2\rangle/M)_\infty$ is consistent with the experimental values of 6.14–6.94 × 10^{-3} nm^2 at 523 K and the *gauche* content of the glycol C–C bond is equal to 76% at some temperature in the range 533–553 K. First, using various values of $E_{\sigma 5}$, $(\langle r^2\rangle/M)$ was calculated for a series of long PET chains (150–200 repeat units) at 523 K and the limiting values $(\langle r^2\rangle/M)_\infty$ determined. (The RIS module from the Accelrys Polymer software [24] using customised versions of the standard statistical weights input files according to the method described previously [1,2] was employed.) The results are shown in Fig. 2, where $(\langle r^2\rangle/M)_\infty$ is plotted against σ_5 for $T = 523$ K. It can be seen that the value of $(\langle r^2\rangle/M)_\infty$ calculated using $E_{\sigma 5} = -4.16$ kJ mol^{-1} is 6.94 × 10^{-3} nm^2, corresponding to the upper value of the range measured experimentally. This was the value of $E_{\sigma 5}$ adopted previously [2] to match $(\langle r^2\rangle/M)_\infty$ at 523 K and to give a gauche proportion of the C–C bond in the glycol unit of 76.4% at the same temperature. It can be seen that a value of $E_{\sigma 5}$ of −5.84 kJ mol^{-1} is needed to reproduce the lower value of $(\langle r^2\rangle/M)_\infty = 6.14 \times 10^{-3}$ nm^2 measured for melts. The Williams–Flory value of $E_{\sigma 5}$ gives $(\langle r^2\rangle/M)_\infty = 9.60 \times 10^{-3}$ nm^2, well outside the experimental values for melts at 523 K.

For given values of $E_{\sigma 5}$ and temperature, proportions of *gauche*$_-$, *trans* and *gauche*$_+$ bond conformers at the C–C bond in the glycol residue were calculated from their *a priori* probabilities, ρ_{g-}, ρ_t, ρ_{g+}, respectively, using the method described previously [1,2]. For various temperatures, the calculated proportions of the various conformers for the C–C bonds in the three central glycol units situated close to the centres of 42-bond PET chains as functions of $E_{\sigma 5}$ are shown in Fig. 3. A chain of 40–42 bonds has been shown previously [2] to be sufficiently long to give the same *a priori* probabilities of the *trans* and *gauche* conformers as infinitely long chains. It can be seen that the original Williams and Flory energy ($E_{\sigma 5} = -1.02$ kJ mol^{-1}) predicts only 61% *gauche* conformers. The modified energy ($E_{\sigma 5} = -4.16$ kJ mol^{-1}), however, predicts 76% *gauche* conformers at 541 K, consistent with the present experimental measurements referring to a melt temperature in the range 533–553 K.

The highest points in Fig. 3, giving proportions of *gauche* conformers ≈81–83%, correspond to $E_{\sigma 5} = -5.84$ kJ × mol^{-1} and $(\langle r^2\rangle/M)_\infty = 6.14 \times 10^{-3}$ nm^2 at 523 K. It can be seen that these proportions are too high, so this value of $(\langle r^2\rangle/M)_\infty$ derived from Guinier analysis of the neutron scattering data can be rejected. The values of $E_{\sigma 5}$ consistent with the measured *gauche* proportion of 76% at melt temperatures of 533 and 553 K are −4.13 kJ mol^{-1} and −4.26 kJ mol^{-1}, respectively, giving values of $(\langle r^2\rangle/M)_\infty$ at 523 K of 6.97 × 10^{-3} nm^2 and 6.91 × 10^{-3} nm^2. These values of $(\langle r^2\rangle/M)_\infty$ are not significantly different from the experimentally measured value at 523 K of 6.94 × 10^{-3} nm^2. Thus, $E_{\sigma 5} = -4.16$ kJ mol^{-1}, which is consistent with this value, is adopted in the present work.

6. Modelling chain conformational behaviour and elastic free-energy

In the first stage of the Monte-Carlo (MC) calculations, the RIS PET chain model is used to generate radial end-to-end distance distribution functions, $W(r)$, for unperturbed chains of various numbers of skeletal bonds (n) at a given temperature. The populations of conformations are generated using conditional probabilities to grow chains bond-by-bond linked with Metropolis acceptance criteria for efficient sampling [25,26]. The radial end-to-end distributions are constructed as histograms for the MC samples generated.

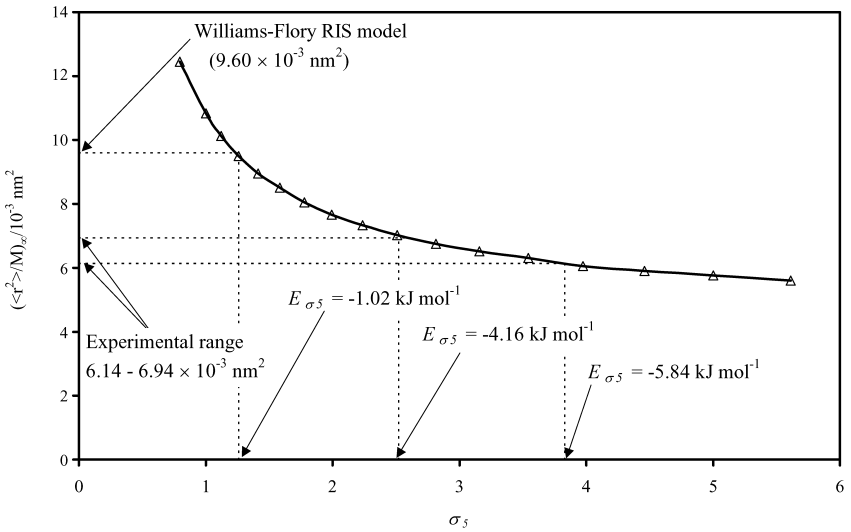

Fig. 2. Characteristic ratio $(\langle r^2\rangle/M)_\infty$ at 523 K plotted against σ_5, the independent statistical weight of *gauche* states of the C–C bond in the glycol segment of PET.

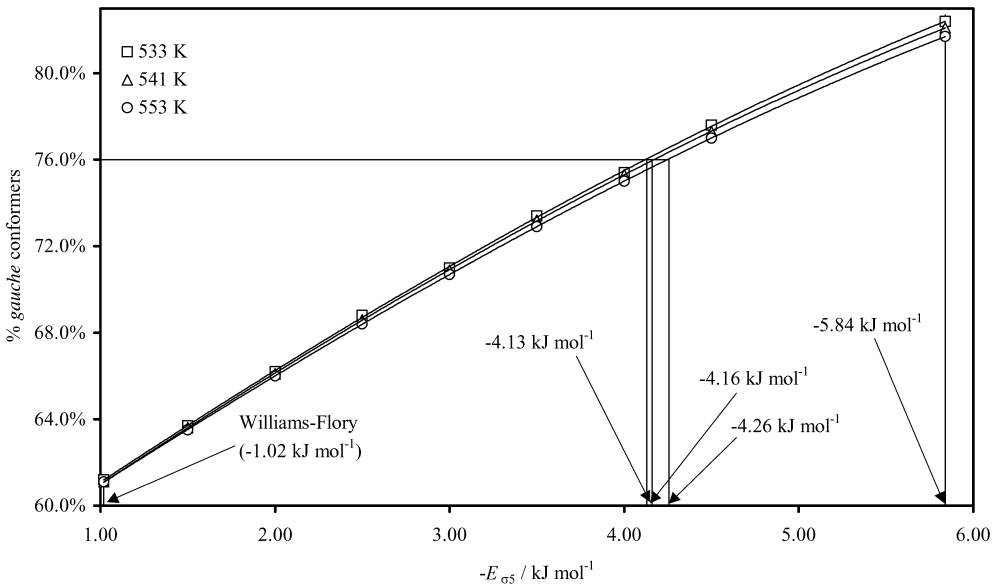

Fig. 3. Proportion of *gauche* conformers of the C–C bond in the glycol segment of PET plotted against $-E_{\sigma 5}$, its bond rotational energy at 533, 541 and 553 K.

The corresponding values of probability density functions $P(\boldsymbol{r})$, are evaluated using

$$P(\boldsymbol{r}) = \frac{W(r)}{4\pi r^2}, \tag{12}$$

assuming the random orientation of chains in three dimensions.

The second stage of the simulations concerns the elastic behaviour of networks. A network is represented by a sample of independent, spherically-symmetrical individual chains in a Cartesian laboratory-reference frame; one end of each chain is fixed at the origin. The chains are deformed uniaxially by a deformation ratio, λ, with $\lambda_x\lambda_y\lambda_z = 1$ (i.e. constancy of volume). The end-to-end distances are allowed to increase only up to their effective, conformational maximum, $r^*_{\max}$, above which $W(r) = 0$ according to the sampled $W(r)$. For an individual polymer chain in a network, the Helmholtz energy change upon deformation at an absolute temperature, T, is assumed to arise solely from the corresponding entropic change. Hence,

$$\Delta A_{\text{chain}}/kT = \ln\{P(r_o)/P(r_{\text{def}})\}, \tag{13}$$

where the subscripts 'o' and 'def' denote the relaxed and deformed end-to-end vectors, respectively.

In the deformation scheme, a chain with end-to-end distance r_o is first chosen in proportion to $W(r_o)$. The X- and Y- co-ordinates of its 'free' chain end are chosen randomly consistent with $x_o^2 + y_o^2 \le r_o^2$ and the Z-component defined consistent with $r_o^2 = (x_o^2 + y_o^2 + z_o^2)$, where the end-to-end vector $r_o = (x_o, y_o, z_o)$. Uniaxial deformations, using a series of values of λ are applied in the Z-direction (i.e. $\lambda = \lambda_z$) and the deformed end-to-end distances calculated by simple geometry, with $\lambda_x = \lambda_y = 1/\sqrt{\lambda}$. Any values of r_{def} in excess of $r^*_{\max}$ are put equal to $r^*_{\max}$, thus limiting r to the range of values consistent with the sampled $W(r)$. The value of $W(r_{\text{def}})$ is ascertained from $W(r)$, and $\ln P(r_{\text{def}})$ evaluated from Eq. (12). The Helmholtz energy change is evaluated via Eq. (13), and the average change per chain at each λ calculated as

$$\Delta A/NkT = \frac{1}{N}\sum_{i=1}^{N} \ln\{P(r_o)/P(r_{\text{def}})\}, \tag{14}$$

where N is the number of chains in the MC sample (i.e. network).

7. Probability density distribution functions ($P(r)$)

The conventional Kuhn treatment [27] is used to compare PE and PET chains. The equivalent freely-jointed chain (m links of length l') is forced to adopt the same mean-square and maximum end-to-end distance, $\langle r^2\rangle$ and $r_{\max}$, as those of the real chain (of n skeletal bonds) with

$$\langle r^2\rangle = ml'^2 \tag{15}$$

$$r_{\max} = ml' \tag{16}$$

Eqs. (15) and (16) allow m to be evaluated from

$$m = \frac{r^2_{\max}}{\langle r^2\rangle} \tag{17}$$

Chains with similar values of m are expected to have similar density distribution functions. Fig. 4 shows $\ln P(\boldsymbol{r})$ vs. $(r/r_{\max})^2$ for PET chains of 84- and 150-bonds and a PE chain of 150-bonds, with $P(\boldsymbol{r})$ evaluated from $W(r)$ using Eq. (12). $W(r)$ for PE and PET were generated [26,28] using histograms divided into 20 and 200 intervals, respectively, between $r = 0$ and $r = r_{\max}$. As discussed previously [28], 200 histogram intervals are required for PET to account accurately for the initial and final curvatures in $W(r)$. The

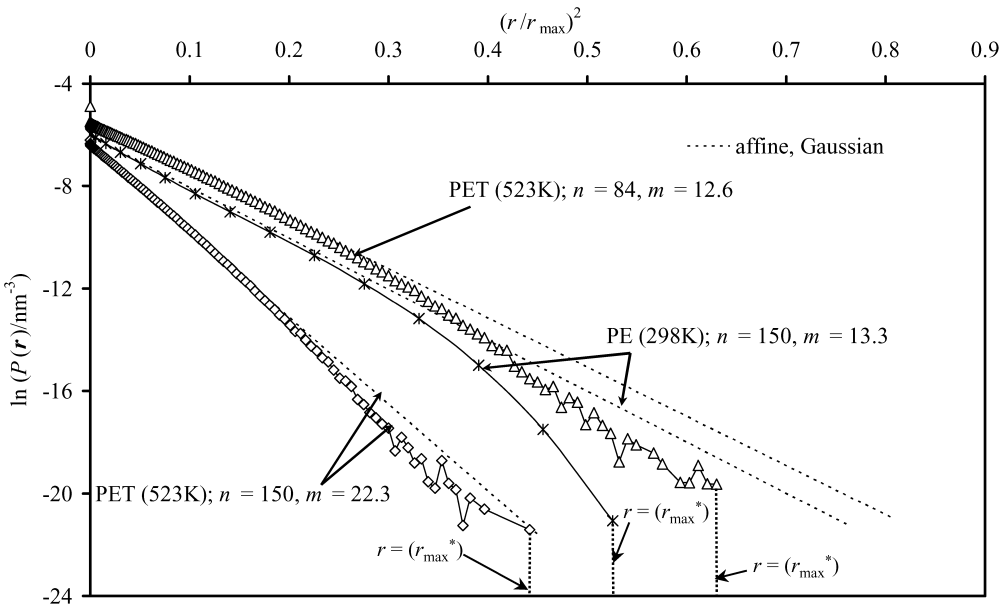

Fig. 4. $\ln P(r)$ vs. $(r/r_{max})^2$ for PET chains of 84 and 150 bonds at 523 K and PE chains of 150 bonds at 298 K.

curvature is caused by the conformational flexibility around the long virtual bond (l_2), giving 50% *cis* and *trans* conformations of the chain about the terephthaloyl unit (see Fig. 2).

Considering first the behaviour as $r \rightarrow 0$, the distributions give the values of $\ln(P(\boldsymbol{r}))$ at $\boldsymbol{r} = 0$ expected from the equivalent Gaussian distributions, namely,

$$(P(\boldsymbol{r}))_{\text{Gaussian}} = \left(\frac{3}{2\pi\langle r^2\rangle}\right)^{3/2} \exp\left(\frac{-3r^2}{2\langle r^2\rangle}\right) \tag{18}$$

with $\ln P(\mathbf{0}) = \ln(3/2\pi\langle r^2\rangle)^{3/2}$.

As r increases towards r^*_{max}, the PET distributions show some undulations. As discussed previously [28], this behaviour may be attributed to the effects of the large flexible virtual bond in the PET structural unit giving relatively higher and lower probabilities at particular values of r. The PE distribution ($n = 150$, $m = 13.3$) also drops more steeply and finishes at a lower value of r/r_{max} than that for the PET distribution for $n = 84$ ($m = 12.8$). It should be recalled that the distributions finish when $r = r^*_{max}$, with r^*_{max} the largest simulated value of r for which $W(r) > 0$.

The steeper slope in Fig. 4 from the PE distribution means that, compared with the PET chain having a similar value of m, there will be a larger drop in entropy and a larger increase in free energy (cf. Eqs. (12) and (13)) as a chain is extended between two given values of $(r/r_{max})^2$. The effects of these differences will be apparent in the following sections when changes in Helmholtz energy resulting from network deformation are considered.

The normalised probability density function $-\ln(P(\boldsymbol{r})/(3/2\pi\langle r^2\rangle)^{3/2})$ is plotted vs. $3r^2/2\langle r^2\rangle$ in Fig. 5 for the same chains as shown in Fig. 4. This normalisation makes it easier to compare deviations from Gaussian behaviour because such behaviour is represented by a universal line of slope equal to 1. For chains of 150-bonds, it can be seen that there is greater deviation from Gaussian behaviour for PE ($m = 13.3$) than for PET ($m = 22.6$). However, when the 150-bond PE chain is compared with a PET chain of 84-bonds ($m = 12.8$) the deviations from Gaussian behaviour are found to be very similar, with the PE showing slightly more deviations. As expected, within the PET chains, deviations decrease as m increases.

8. Helmholtz energy change

The network Helmholtz energy change accompanying a macroscopic uniaxial deformation of λ, with no volume change, can be expressed as [25,26]

$$\Delta A/NkT = s(\lambda^2 + 2/\lambda - 3). \tag{19}$$

For Gaussian (affine) networks [27], $s = 1/2$, and a plot of $\Delta A/NkT$ vs. $\lambda^2 + 2/\lambda - 3$ for uniaxial extension and compression is linear with a slope of 1/2.

As far as the changes in Helmholtz energy are concerned, the non-affine network chain behaviour described previously [25,26,28] can be viewed as a kind of orientation effect. Chains in the relaxed network, whose end-to-end vectors lie close to the extension axis become conformationally fully extended at low macroscopic strains, and hence contribute nothing more to the Helmholtz energy change of the network as deformation increases further; more of the strain is effectively 'taken-up' by network chains whose end-to-end vectors lie at ever-increasing angles from the extension axis. The phenomenon manifests itself as a reduction in the rate of Helmholtz energy change per chain with increasing macroscopic deformation.

The energy changes on deformation to given values of λ

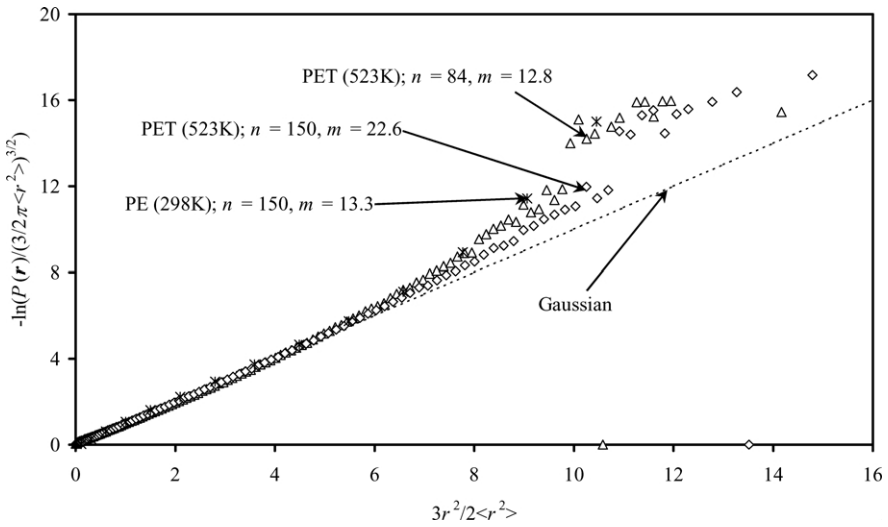

Fig. 5. $-\ln(P(\mathbf{r})/(3/2\pi\langle r^2\rangle)^{3/2})$ vs. $3r^2/2\langle r^2\rangle$ for PET chains of 84 and 150 bonds at 523 K and PE chains of 150 bonds at 298 K.

were evaluated using Eq. (14). The results in extension are shown vs. $\lambda^2 + 2/\lambda - 3$ in Fig. 6 and those in compression in Fig. 7. Results for PET networks of 60-, 84-, 108- and 150-bond chains and for PE networks of 60- and 150-bond chains are shown. Overall, there are smaller deviations from Gaussian behaviour in compression than in extension. Also, the PET networks show smaller deviations than the PE networks and ΔA is less sensitive to chain length. Such comparative behaviour is consistent with the distribution functions of Figs. 4 and 5, in that the slopes of the PET curves are nearer to the Gaussian slopes than is the slope of the PE curve. The contributions from individual chain deformations that are summed to give ΔA (Eq. (14)) are equal to differences in ordinates between pairs of points on the curves shown in Fig. 4. Hence, deviations from Gaussian behaviour in ΔA relate to the differences between the slopes of the curves in Figs. 4 and 5 and the slopes of the Gaussian lines. However, it should be remembered that the whole network has to be considered as there is not a unique relationship between the slope and ΔA because r for an individual chain and λ can subtend any angle to each other and, in addition, extension of an individual chain beyond $r = r^*_{\max}$ cannot occur.

Generally, at small deformations, chains show larger Helmholtz energy changes than those expected for freely-jointed Gaussian chains. As deformation increases and some chains reach conformational full extension, the rate of change of Helmholtz energy decreases and eventually, in all cases, ΔA will fall below the Gaussian values. Inspection of the results in Figs. 6 and 7 show that shorter PET chains start with higher values of ΔA. In all cases, if the range of the abscissae were increased to larger λ, the values of ΔA would, as more chains become fully extended, eventually lie below the Gaussian line and in fact be smaller for shorter chain lengths. The curves plotted for the stiffer PE chains lie above those for the PET chains at smaller deformations but

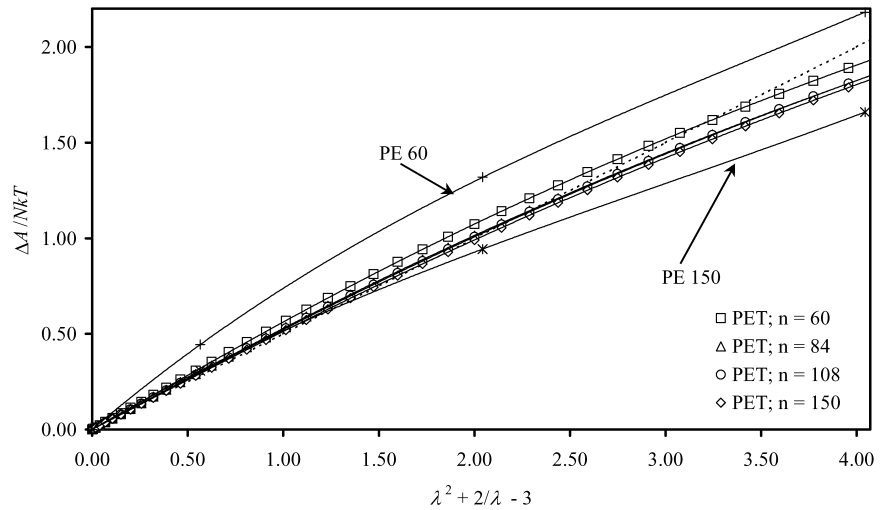

Fig. 6. Helmholtz energy change per chain ($\Delta A/NkT$) as a function of $\lambda^2 + 2/\lambda - 3$ for networks of PET chains of 60, 84, 108 and 150 skeletal bonds at 523 K and for networks of PE chains of 60 and 150 skeletal bonds at 298 K under uniaxial extension.

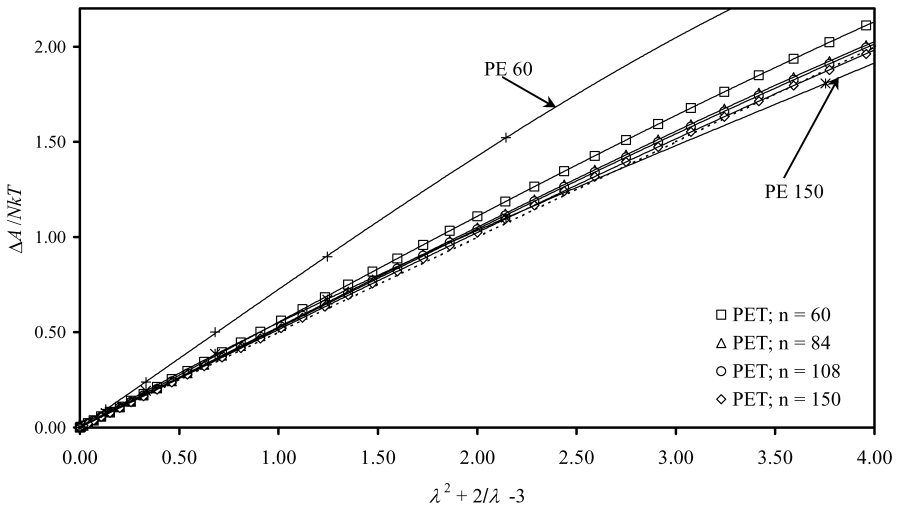

Fig. 7. Helmholtz energy change as a function of $\lambda^2 + 2/\lambda - 3$ for networks of PET chains of 60, 84, 108 and 150 skeletal bonds at 523 K and for networks of PE chains of 60 and 150 skeletal bonds at 298 K under uniaxial compression.

show larger decreases in their rates of change of ΔA with deformation, so that as deformation increases the curve for PE, $n = 150$, falls below those for the PET chains.

9. Stress–strain behaviour

The normalised Helmholtz energy change in Eq. (19) can be expressed [25,26] in terms of the density, ρ, and volume, V, of the unswollen network:

$$\frac{\Delta A}{RT\rho}\frac{1}{V} = \frac{s}{M_c}(\lambda^2 + 2/\lambda - 3) \tag{20}$$

where R is the universal gas constant and M_c is the network-chain molar mass. In general, s is a function of λ. Differentiation of Eq. (20) with respect to sample length, l, yields the normalised retractive force, $f/RT\rho$:

$$\frac{f}{RT\rho}\frac{1}{V} = \frac{1}{l_o M_c}\left[2s(\lambda - 1/\lambda^2) + (\lambda^2 + 2/\lambda - 3)\frac{ds}{d\lambda}\right] \tag{21}$$

where l_o is the initial sample length. The normalised, nominal stress, $\sigma/RT\rho$, can then be found by using the relationship $a_o l_o = V$, where a_o is the initial sample cross-sectional area. Thus,

$$\frac{\sigma}{RT\rho} = \frac{f}{RT\rho a_o} = \frac{1}{M_c}\left[2s(\lambda - 1/\lambda^2) + (\lambda^2 + 2/\lambda - 3)\frac{ds}{d\lambda}\right] \tag{22}$$

The values of $\sigma/RT\rho$ can be converted [25–28] to reduced normalised stress, $[\sigma^*]/RT\rho$, with

$$\frac{[\sigma^*]}{RT\rho} = \frac{\sigma}{RT\rho(\lambda - 1/\lambda^2)}. \tag{23}$$

Plots of $[\sigma^*]/RT\rho$ vs. $1/\lambda$ give Mooney–Rivlin plots. The reduced normalised stress (reduced modulus) for an affine, Gaussian network is equal to $1/M_c$ and is constant at all λ (in Eq. (22) $s = 1/2$ and $ds/d\lambda = 0$). Fig. 8 shows the Mooney–Rivlin plots for the PET networks and for the 150-bond PE network. (The 60-bond PE network is not shown because the expanded scale required would reduce the clarity with which the other results can be shown.) In each case, the intercept at $\lambda = 1$, is greater than the Gaussian value. This behaviour follows directly from the initial values of ΔA in Fig. 6 being larger than the Gaussian values. The intercepts tend towards the Gaussian values as chain length increases.

In Fig. 9, $[\sigma^*]/RT\rho$ is further normalised by multiplying by M_c and is plotted vs. $1/\lambda$. Again the 60-bond PE network is omitted for clarity. The resultant curves better illustrate deviations from affine, Gaussian behaviour, with the affine, Gaussian value being equal to 1 at all values of $1/\lambda$ for all chain lengths. Apart from networks of the shortest chain of 60-bonds, the curves for the PET networks are closer to the affine, Gaussian value than that for the PE network. Within the PET networks, curvature decreases as chain length increases and deviations from affine, Gaussian behaviour again decrease as chain length increases.

Comparison between PE and PET is clearer on the basis of Fig. 10 where, for the same networks as Figs. 8 and 9, the effect is shown of dividing $\{[\sigma^*]/RT\rho\}M_c$ by 2 s, twice the initial slopes of the curves in Fig. 6. This further normalisation to remove the differences due to deviations from limiting Gaussian behaviour is useful because it allows comparison of the deviations of the networks from affine behaviour alone ($ds/d\lambda \neq 0$). Results for a 60-bond PE network are also plotted in this figure. It can be seen that the two PE networks have curves distinct from those for the PET networks. They show deviations from affine behaviour at values of λ nearer to 1 ($1/\lambda \approx 0.95$) than do the PET networks for which deviations become apparent at $1/\lambda \approx 0.85$. In general, for a given chain structure, longer-chain networks deviate less from affine behaviour than do

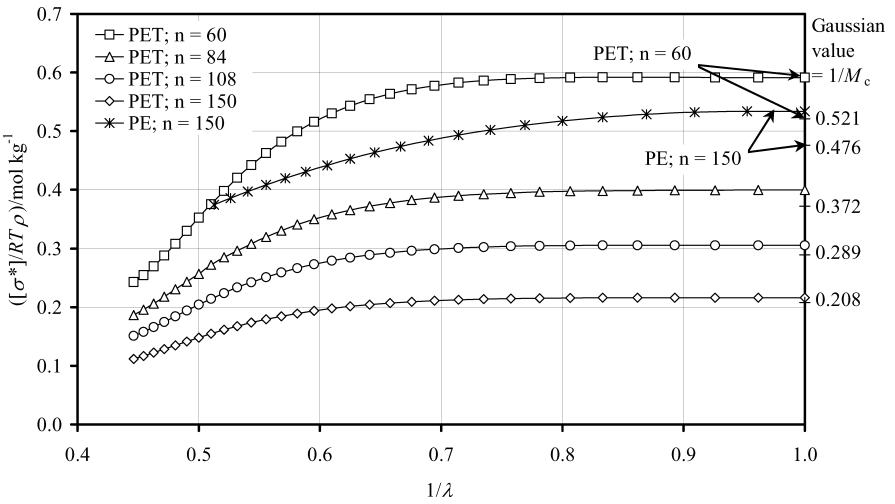

Fig. 8. Mooney–Rivlin plots for networks of PET chains of 60, 84, 108 and 150 skeletal bonds at 523 K and for a network of PE chains of 150 skeletal bonds at 298 K. The values predicted by affine, Gaussian behaviour ($s = 1/2$ and $ds/d\lambda = 0$), namely, $[\sigma^*]/RT\rho = 1/M_c$, are indicated on the right-hand ordinate.

shorter-chain networks. This trend results from larger proportions of the shorter chains becoming conformationally fully-extended. The different shapes of the curves for the PET and PE chains show that the new type of plot proposed in Fig. 10 is useful for characterising the effects of chain structure on stress–strain behaviour, independent of network chain molar mass.

10. Summary and further work

First, the accurate IR spectrometry measurements described in the present paper establish the RIS model for PET melts as having the rotational energy difference of -4.16 kJ mol^{-1} between *trans* and *gauche* states for the glycol residue. Second, by using the MC method and RIS models of network chains, one is able to explain stress–strain behaviour in relation to chemical structure. This has now been demonstrated for PE, PDMS and PET networks. The plots in Figs. 8, 9 and 10 show clearly that networks of PET chains have lower moduli and smaller deviations than those of PE chains of similar numbers of equivalent freely-jointed links. The distinction arises from the greater conformational flexibility of the PET chain structure, notwithstanding the effects of the long (virtual) bond bridging the benzene ring in PET on $W(r)$ and $P(r)$ at small and large values of r. New normalised Mooney–Rivlin plots (Figs. 9 and 10) are introduced to characterise deviations from affine, Gaussian behaviour for different chain structures.

Subsequent publications will apply the present results to modelling the measured stress–strain behaviour of PET melts and will further develop the MC method to interpret their stress-optical properties. The conformational properties due specifically to the long virtual bond in the PET chain also need further investigation.

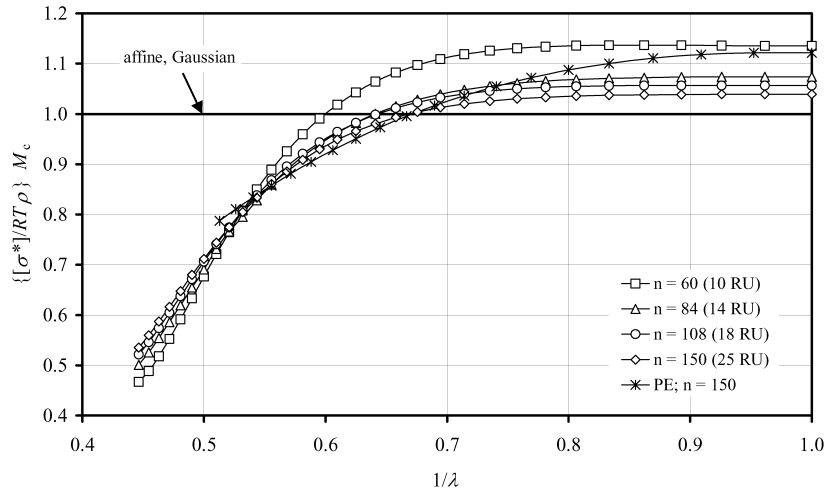

Fig. 9. $\{[\sigma^*]/RT\rho\}M_c$ vs. $1/\lambda$ for networks of PET chains of 60, 84, 108 and 150 skeletal bonds at 523 K and for a network of PE chains of 150 skeletal bonds at 298 K. The value predicted by affine, Gaussian behaviour is indicated.

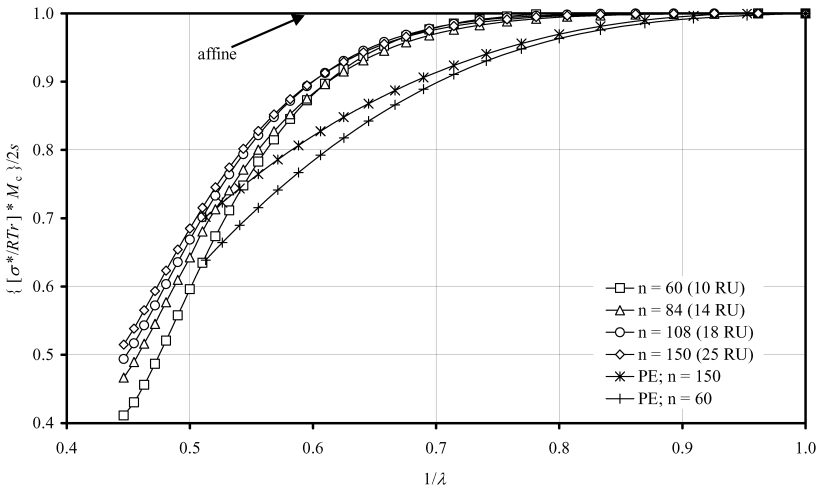

Fig. 10. $\{[\sigma^*]/RT\rho\}M_c/2$ s vs. $1/\lambda$ for networks of PET chains of 60, 84, 108 and 150 skeletal bonds at 523 K and for a network of PE chains of 60 and 150 skeletal bonds at 298 K. $\{[\sigma^*]/RT\rho\}M_c/2s = 1$, the value predicted by affine behaviour ($ds/d\lambda = 0$) is indicated.

Acknowledgements

The support of the EPSRC is gratefully acknowledged and also access to the Accelrys Polymer software for the background RIS calculations. We also wish to thank Dr Alison Voice for helpful advice with regard to analysing the infrared data.

References

[1] Taylor DJR, Stepto RFT, Bleackley M, Ward IM. Phys Chem Chem Phys 1999;1:2065.
[2] Cail JI, Stepto RFT, Taylor DJR, Jones RA, Ward IM. Phys Chem Chem Phys 2000;2:4361.
[3] Williams AD, Flory PJ. J Polym Sci 1967;5(A-2):417.
[4] Gilmer JW, Wiswe D, Zachmann H-G, Kugler J, Fischer EW. Polymer 1986;27:1391.
[5] Heffelfinger CJ, Schmidt PG. J Appl Polym Sci 1965;9:2661.
[6] Cunningham A, Ward IM, Willis A, Zichy V. Polymer 1974;15:749.
[7] Yazdanian M, Ward IM. Polymer 1985;26:1779.
[8] Shen D, Long F, Wen Z, Qian R. Makromol Chem 1991;192:301.
[9] Spiby P, O'Neill MA, Duckett RA, Ward IM. Polymer 1992;33:4479.
[10] Guévremont J, Ajji A, Cole KC, Dumoulin MM. Polymer 1995;36:2285.
[11] Rodríguez-Cabello JC, Merino JC, Quintanilla L, Pastor JM. J Appl Polym Sci 1996;62:1953.
[12] Green DI, Bower DI. Spectrochim Acta 1993;49A(8):1191.
[13] Thermo Galactic, 395 Main Street, Salem, NH 03079 USA.
[14] Yazdanian M, Ward IM, Brody H. Polymer 1985;26:1779.
[15] Hutchinson IJ, Ward IM, Willis HA, Zichy V. Polymer 1980;21:55.
[16] Spiby P. PhD Thesis, University of Leeds, 1988.
[17] Middleton AC. PhD Thesis, University of Leeds, 1997.
[18] Abell L. PhD Thesis, University of Leeds, 1995.
[19] Cunningham A, Davies GR, Ward IM. Polymer 1974;15:743.
[20] Ward IM. Chem Ind 1956;905.
[21] Ward IM. Chem Ind 1957;1102.
[22] Grime D, Ward IM. Trans Faraday Soc 1958;54:959.
[23] Lapersonne P, Bower DI, Ward IM. Polymer 1992;33:1277.
[24] Accelrys, 9685 Scranton Road, San Diego, CA 92121, USA.
[25] Stepto RFT, Taylor DJR. Macrolmol Symp 1995;93:261.
[26] Stepto RFT, Taylor DJR. J Chem Soc Faraday Trans 1995;91:2639.
[27] Treloar LRG. The physics of rubber elasticity, 3rd ed. Oxford: Oxford University Press; 1975.
[28] Cail JI, Stepto RFT. Polymer 2003;44:6077.